ACS APPLIED MATERIALS & INTERFACES

www.acsami.org

Research Article

Shape-Programmed Fabrication and Actuation of Magnetically Active Micropost Arrays

Jisoo Jeon, Jeong Eun Park, Sei Jin Park, Sukyoung Won, Hangbo Zhao, Sanha Kim, Bong Sup Shim, Augustine Urbas, A. John Hart,* Zahyun Ku,* and Jeong Jae Wie*

Cite This: *ACS Appl. Mater. Interfaces* 2020, 12, 17113−17120

Read Online

ACCESS | Metrics & More | Article Recommendations | Supporting Information

ABSTRACT: Micro- and nanotextured surfaces with reconfigurable textures can enable advancements in the control of wetting and heat transfer, directed assembly of complex materials, and reconfigurable optics, among many applications. However, reliable and programmable directional shape in large scale is significant for prescribed applications. Herein, we demonstrate the self-directed fabrication and actuation of large-area elastomer micropillar arrays, using magnetic fields to both program a shape-directed actuation response and rapidly and reversibly actuate the arrays. Specifically, alignment of magnetic microparticles during casting of micropost arrays with hemicylindrical shapes imparts a deterministic anisotropy that can be exploited to achieve the prescribed, large-deformation bending or twisting of the pillars. The actuation coincides with the finite element method, and we demonstrate reversible, noncontact magnetic actuation of arrays of tens of thousands of pillars over hundreds of cycles, with the bending and twisting angles of up to 72 and 61°, respectively. Moreover, we demonstrate the use of the surfaces to control anisotropic liquid spreading and show that the capillary self-assembly of actuated micropost arrays enables highly complex architectures to be fabricated. The present technique could be scaled to indefinite areas using cost-effective materials and casting techniques, and the principle of shape-directed pillar actuation can be applied to other active material systems.

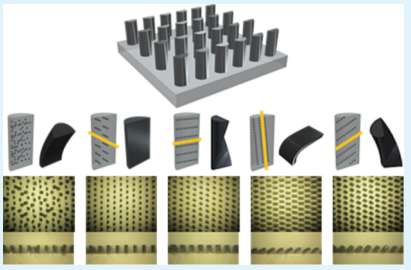

KEYWORDS: *actuation, micropillar, magnetic, wetting, self-assembly*

1. INTRODUCTION

Programmable stimuli-responsive materials have emerged as an attractive candidate for shape-reconfigurable devices and soft robotics, and various stimuli have been used for actuation, such as heat,[1−4] light,[5−9] humidity,[10−12] and magnetic field.[13−16] However, most reconfigurable polymeric systems reported to date are limited in their operating environments. For example, hydrogel or solvent-responsive materials require submersion in liquids, making high-precision localized actuation challenging,[17,18] and thermoresponsive materials often actuate at high temperatures or require a time-consuming cooling process for shape recovery.[19] Optoresponsive materials require exposure to light, which increases the sample temperature by photothermal effects and/or limits the actuation to the surface level because of an exponential intensity decay (described by the Beer−Lambert law) into the material. On the other hand, magnetoresponsive materials can operate at room temperature without the need of submersion in liquids and are expected to have uniform actuation throughout the material.

Recently, magnetic actuation of microarrays has been studied extensively using hard magnet-based polymeric composites with symmetric micropillars.[20−24] Incorporating hard magnets enables magnetic actuation using weak external magnetic fields because of their strong magnetic dipoles. However, magnetic attraction between hard magnetic particles induces nonuniform magnetic actuation because of intermicropillar influences. Conversely, weak magnetic dipoles from soft magnetic particles can reduce undesirable interactions among micropillars at the expense of actuation strain. In this study, we employed soft magnetic particles embedded in polymer matrices and asymmetric micropillar geometry to demonstrate the synchronized multimodal actuation from anisotropic mechanical properties along the actuation direction.

The geometry of micro-/nanoarrays significantly modifies surface properties such as adhesion,[25,26] wettability,[27,28] liquid transport,[21,29,30] and spreading.[31−33] Unidirectional liquid spreading can be achieved using complex microfabrication processes; yet, it remains difficult to create a surface with reversible and/or tunable liquid spreading. In the case of solvent evaporation on nanopillars, capillary forces cause spontaneous deformation and self-assembly.[34] Although capillary force-assisted self-assembly of nanopillars can be used to produce unique three-dimensional (3D) structures which are challenging to replicate via conventional soft

Received: January 25, 2020
Accepted: March 5, 2020
Published: March 5, 2020

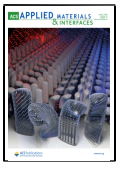

https://dx.doi.org/10.1021/acsami.0c01511
ACS Appl. Mater. Interfaces 2020, 12, 17113−17120

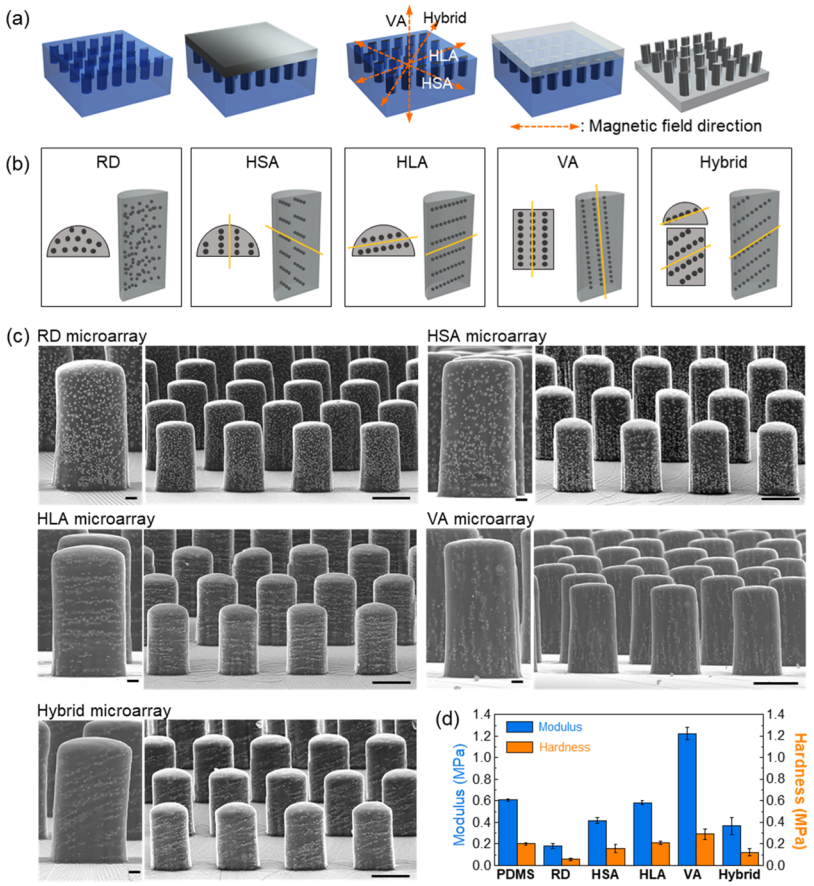

Figure 1. Sample information. (a) Schematic illustration of the preparation of preprogrammed, magnetically responsive microarrays. (b) Different alignment of the magnetic component in microarrays. (c) SEM micrographs of each sample. Scale bars: 5 μm (left), 30 μm (right). (d) Modulus and hardness from the nanoindentation curves by the Oliver−Pharr method (error bars are standard deviations).

lithography, these clustered nanostructures are unable to return to their original configurations after assembly. In this work, we introduce a novel strategy to achieve a large actuation strain with minimum intermicropillar interactions by programming an alignment of soft magnetic iron particles within polydimethylsiloxane (PDMS) matrices. Maximum magnetic torque, thus actuation, will be achieved when the iron particles are aligned perpendicular to the applied magnetic field. However, this will result in random actuation directions; hence, a slight tilt of the iron particle alignment was employed to achieve uniform actuation of the array. Rapid, reversible actuation is demonstrated over hundreds of cycles, without noticeable decay in the actuation strain. Simultaneous multidirectional actuation in a single microarray was achieved using iron particle alignment via multiple magnets or the masking technique. Further, we demonstrate on-demand liquid spreading and reversible self-assembly using the magnetically actuated microarrays.

2. EXPERIMENTAL SECTION

2.1. Preparation of Composite Micropillar Arrays. Magnetic particle, carbonyl iron powder ("CIP", HQ grade, BASF), was mixed with the PDMS precursor ("PDMS", Sylgard 184, Dow Corning) by mechanical mixing at a 10 vol % particle loading. The details of the iron powder are described in the Supporting Information (Figures S1 and S2). The mixture was poured to a hydrophobic coated PDMS-negative micromold which has hemicylindrical holes. For hydrophobic coating, it was placed in a vacuum chamber with trichloro(1*H*,1*H*,2*H*,2*H*-perfluorooctyl)silane (Sigma-Aldrich) for 1 h. The mold with the mixture was located in a vacuum chamber and evacuated for the sufficient filling of the holes. After the filling process, the residual mixture was mechanically removed from the mold. In order to align the magnetic particles within the microstructures, the mold filled with the composite mixture was placed between two 0.12 T neodymium permanent magnets at 50 °C for 3 h. For the uniform directionality of actuation, the magnetic particles were aligned with a tilt angle (~10°). The PDMS mold was placed on the sloped stage for tilted particle alignment. The magnetic particles were immobilized within the PDMS matrix by precuring, resulting in the fixation of the desirable alignment of magnetic components. The PDMS precursor was poured onto the master mold, and PDMS was thermally cured at 80 °C for 2 h. The micropillars on the PDMS substrate were detached from the mold.

2.2. Actuation of Microarrays. To generate and control the external magnetic field, the sample was placed between two neodymium magnets (0.55 T) with a motorized yoke that can control the gap (custom-made, Ecopia, Figure S3a, Supporting Information). The range of the magnetic field is 0.05−0.6 T. The applied magnetic field direction for actuation is parallel to horizontally short axis to top-down view of pillar (Figure S3b, Supporting Information). The actuation of the micropillars was optically visualized and recorded by a videoscope (SV-32, Sometechvision).

2.3. Arbitrary Patterned Microarray. For arbitrary patterning, an imide tape was used for masking the mold. The imide tape cut to the desired pattern was attached to the PDMS-negative mold. After filling the hole with the PDMS−CIP mixture, the residual mixture was removed and the imide tape was detached. Then, the PDMS mold partially filled with the mixture was placed between two 0.12 T neodymium permanent magnets at 50 °C for 3 h. After fixing the magnetic particles via precuring the PDMS matrix, the other holes

https://dx.doi.org/10.1021/acsami.0c01511
ACS Appl. Mater. Interfaces 2020, 12, 17113−17120

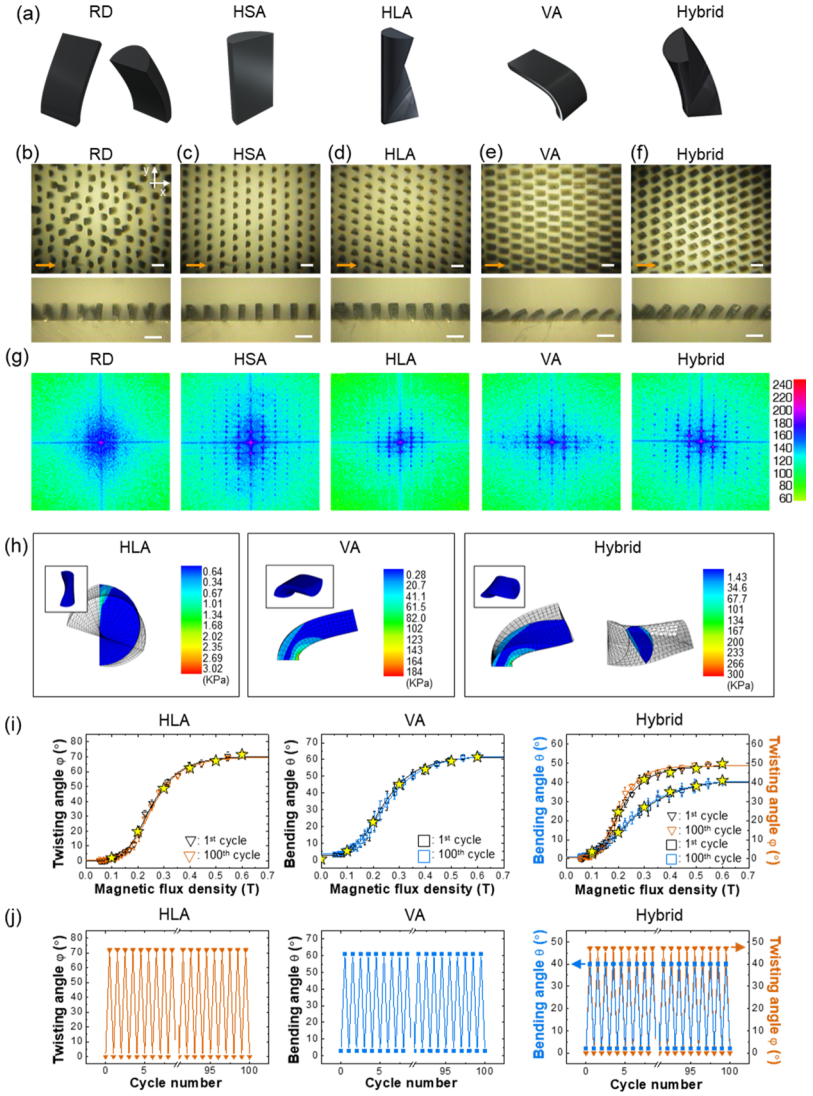

Figure 2. Actuation of each sample and the evaluation of actuation. (a) Schematic illustration of different actuation modes of the micropillar. (b–f) Top-down (upper) and side (bottom) views of micropillar arrays upon actuation (scale bars: 50 μm; (b) RD microarray, (c) HSA microarray, (d) HLA microarray, (e) VA microarray, (f) hybrid microarray). (g) FFT top-down view of each actuation image. (h) Von Mises stress distribution within the structures with the deformed geometries by FEM simulation. (i) Comparison between simulation and measured bending, torsion, and bending and torsion angles of 1st cycle and 100th cycle. Yellow stars indicate the simulation data (error bars are standard deviations). (j) Repeatability of magnetic actuation of microarrays between 0.05 and 0.6 T.

were filled with the PDMS–CIP mixture. After removing the residual mixture, the PDMS matrix was precured between two neodymium permanent magnets at 50 °C for 3 h. The PDMS precursor was poured to the master mold, and PDMS was cured at 80 °C for 2 h. The micropillars on the PDMS substrate were detached from the mold.

2.4. Solution for Liquid Spreading and Self-Assembly. Solutions composed of deionized water, hand soap, and colorant (JEY'S F. I. Inc, Lac colorant L) were prepared with 80:10:10 for liquid spreading and 89.5:10:0.5 for self-assembly, respectively. The solution (about 0.5 μL) was dropped on each actuated microarray using a micropipette. The applied magnetic field was 0.6 T. The self-assembled microarray was dried in ambient condition for 24 h.

2.5. Material Characterization. Scanning electron microscopy (SEM) micrographs were captured by a scanning electron microscope (S-4300, Hitachi).

Nanoindentation was performed by a nanoindenter (TI900, Hysitron) using a sapphire indenter with a 10 μm diameter. The tip was indented at the center of five different pillars on the same sample to a maximum depth of 4500 nm at a 100 nm/s of indentation rate and 3 s of stoppage between loading and unloading. The modulus is determined from the unloading curves by the Oliver–Pharr method, and the hardness is determined by the maximum force before unloading divided by the contact area.

3. RESULTS AND DISCUSSION

3.1. Programming Magnetoactuation of Polymer Composite Microarrays. Magnetically active microarrays are prepared by replica molding of PDMS–iron particle composites, and the alignments of iron particles according to the directions of the magnetic field during precuring are depicted in three-dimensional schemes (Figure 1a, details in the Experimental Section). The iron particles are arranged in one of the following ways: randomly dispersed (RD), horizontal short-axis aligned (HSA), horizontal long-axis aligned (HLA), vertically aligned (VA), and combination of HLA and VA (hybrid) (Figure 1b), confirmed by SEM images (Figures 1c and S4, Supporting Information). Nanoindentation corroborates the alignment-dependent mechanical compliance

https://dx.doi.org/10.1021/acsami.0c01511
ACS Appl. Mater. Interfaces 2020, 12, 17113–17120

and uniformity of the microarrays. As expected, the samples with iron particles aligned perpendicular to the applied load exhibit the highest modulus and hardness (Figure 1d and S5, Supporting Information). The introduction of magnetic particles may impede the cross-linking density of PDMS;[35] therefore, the composite micropillars are more compliant than pure PDMS, except the VA microarrays. The greater stiffness of the VA microarrays is due to the well-aligned particles toward the direction of indentation, which can partly support the indenting force.

The programmed microarrays are actuated by locating the microarrays between two permanent magnets on motorized stages of a custom-built setup that controls the separation and angle of the magnets (Figure S3a, Supporting Information). Magnetic flux densities ranging from 0.05 to 0.60 T are used, and the field direction is along the short axis of the semicylindrical micropillars unless noted otherwise (Figure S3b, Supporting Information). The actuation of each microarray is schematically illustrated in Figure 2a. For RD microarrays, random bending directions with nonuniform amplitudes are observed (Figure 2b). When the alignment of iron particles is parallel to the external magnetic field (HSA microarray), no array deformation is observed as the magnetic torque is zero (Figure 2c). On the other hand, perpendicular alignment of the iron particles to the magnetic field (HLA microarray) causes significant magnetic torsion, resulting in a uniform twisting of micropillars (Figure 2d). The twisting of semicylindrical micropillars induces readily visible optical changes of the surface (whereas full cylindrical micropillar twisting would not). The VA microarray also has a perpendicular alignment with respect to the B field; however, the iron particles are aligned along the height of the micropillar (Figure 2e). We found that VA micropillars have no preferential bending direction, as seen in Figure S6, Supporting Information In order to establish a preferential bending direction, the iron particles are aligned at a slight (~10°) tilt with respect to the pillars' height axis. In doing so, uniform bending is achieved over large-area microarrays. Finally, we successfully demonstrate simultaneous torsion and bending in the hybrid arrays by setting the iron particle alignment in between HLA and VA directions (Figure 2f).

The structural deformation of the actuated micropillars is modeled using the finite element method (FEM) by discretizing the deformation sequence, iteratively updating the forces acting on the geometry and solving for the deformation. This approach captures the intermediate geometries that influence the final deformation[36] and reflects the experimental results well (for more information on the FEM simulation, refer to Figures S7−S9, Supporting Information). Figure 2h shows the Von Mises stress distribution within the structures, with the deformed geometries shown in insets for the bending, twisting, and hybrid structures. The Von Mises stress is a representation of the complex stress state when the material will be in during actuation, which will lead to failure if its value exceeds the material's yield strength. The maximum Von Mises stresses calculated are well below the yield strength of the PDMS matrix, and therefore no structural failure is expected;[36] indeed, no such failures are observed during experiments. For twisting structures, the stress is mostly concentrated around the upper half of the vertical edge of the base plane. For bending structures, the stress distribution on the vertical midplane is shown, and the highest stress values are found at the base in the direction of bending. For hybrid structures, stress distributions of both the vertical midplane and the horizontal midplane are shown. Because the hybrid actuation is a combination of bending and twisting, similarities to both are observed. In the vertical midplane, the highest stresses are concentrated at the base toward the bending direction. In the horizontal midplane, the highest stress values are around the upper half of the straight edge, with additional stress concentrations around the semicircular edge. In addition, the uniformity and directionality of the actuated micropillar arrays are proved by the fast Fourier transforms (FFTs) (Figure 2g).

We also found that the magnetoactuation of HLA, VA, and hybrid microarrays is highly repeatable over a hundred cycles. Remarkably, the actuation angle stays constant over a hundred cycles within error, at actuating magnetic flux densities of 0.2−0.4 T, and the saturation angle of each actuation mode also remains the same (HLA twisting: 72°, VA bending: 61°, hybrid twisting: 49°, hybrid bending: 40°), as shown in Figure 2i. The VA microarray has a noticeable bending angle at magnetic flux densities as low as 0.05 T because of the large magnetic moment of the aligned particles. The Hill equation can be employed to describe the S-shaped actuation responses of each mode, depending on the actuating magnetic flux density. It successfully describes the actuation angles at the 1st and 100th cycles for each mode, confirming the excellent repeatability of the magnetic actuation (Figure 2i and Movies S1−S5, Supporting Information). The magnetic hysteresis was found to be insignificant during the reverse scan (0.6−0.05 T) (Figure S10, Supporting Information). In addition, the minimum and maximum actuation angles are identical during the cycles without permanent deformation (Figure 2j).

Multimodal magnetic actuation of the micropillar arrays was achieved by rotating the arrays relative to the linear external magnetic field. The bending stiffnesses ($k = 3EI/L^3$) of the semicylindrical micropillars change according to the offset angle and are minimized when the bending direction is parallel to the horizontal short axis (Figure S11, Supporting Information), where E is the elastic modulus of materials, I is the second moment of inertia, and L is the length of the micropillars. Therefore, more micropillars bend when the applied magnetic field is parallel to the horizontal short axis (Figure S12, Supporting Information). On the other hand, HSA and HLA microarrays have torsional stiffnesses independent of the twisting direction, and only the alignment axis of the iron particles affects the magnetic torsion (Figures S13 and S14, Supporting Information). The bending angle of VA and hybrid microarrays becomes larger when the bending direction approaches the horizontal short axis owing to the decrease of the bending stiffness (Figures S15 and S16, Supporting Information).

3.2. Concerted Actuation Modes in a Single Sample.

In addition to the uniform actuations over a large area, we sought to achieve concerted actuation modes in a single sample. A quadripolar magnetic array was employed to spatially program the magnetic field directions and alignment of magnetic particles within the polymer matrices, as shown in Figure S17, Supporting Information The detailed spatial distribution of the magnetic field information was simulated using a magnetic field simulator (ANSYS discovery AIM R19.2) (Figure 3a). The cross sections of the 3D magnetic field along the black and red dashed lines from the top-down view of the magnetic field (Figure 3a(i)) are shown in Figure 3a(ii,iii). Note that the negative PDMS mold is located at the

https://dx.doi.org/10.1021/acsami.0c01511
ACS Appl. Mater. Interfaces 2020, 12, 17113−17120

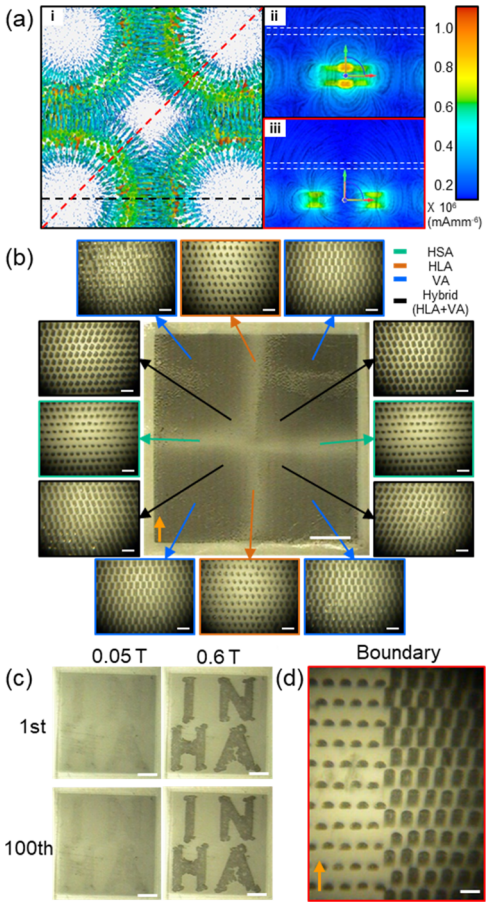

Figure 3. Concerted actuation in a single microarray. (a) Simulation of magnetic field intensity and direction. (i) Top-down magnetic field scheme of quadripolar array; (ii, iii) diagonal cross-sectional magnetic field scheme (each outline color corresponding to the dotted line in a-i); 3D arrows are the directions of the magnetic field and the white dotted line is the location of the negative mold when aligning the magnetic particles. (b) Image of concerted actuation (no actuation, twisting, bending, and bending and twisting) in a single sample (scale bars: center image—2 mm, zoomed image—50 μm). (c) Before (left) and after (right) actuation of VA arbitrary patterned microarray (INHA letters; letter: VA; background: HSA, scale bars: 2 mm). (d) Zoomed image of the boundary between the letter and background at 0.6 T (scale bars: 50 μm).

white dotted line, and the quadripolar magnetic arrays are placed at the bottom of the PDMS-negative mold (Figure S1c, Supporting Information) instead of the linear magnetic field. After polymerization, the quadripolar magnetic array was removed, and the magnetic actuation was performed by a linear external magnetic field as previously described. The offset angle between the magnetic alignment of iron particles and the linear external magnetic field determines the modes of actuation, and a clearly varying optical reflectance arising from the concerted actuation modes was observed (Figure 3b and Movie S6, Supporting Information).

Although the multiple magnet setup allows concerted actuation modes in a single array, the magnetic field design is limited by the magnet's sizes. To program magnetic actuation modes in arbitrary patterns, we masked certain areas on the mold to selectively fill the mold with the PDMS/CIP mixture and carried out the alignment of magnetic particles (Figure S18; details in the Experimental Section, Supporting Information). In the presence of an external magnetic field, a grayscale color difference from the top-down view is induced by the different surface coverage of the actuated micropillar which has dark color from the iron particles (Figure S19 and Table S1, Supporting Information). Especially, the obvious optical difference is obtained by using the inert mode with other actuation modes owing to the minimized surface coverage change. One such array is shown in Figure 3c and Movie S7, Supporting Information, and the letters "INHA" are revealed upon magnetoactuation because of the difference in the optical transmittance of the bent VA microarrays (covering the letters) and pristine HSA microarrays (covering the surrounding areas). The masking technique provides the sharp boundaries of the magnetic actuation modes clearly shown in the bulk microarrays (Figure 3d). In the case of twisting mode, the optical difference is observed in tilted view owing to twisting-induced rotation of the thicker surface of semicylindrical shaped micropillar to viewpoint (Figure S20b,b′, Supporting Information). Hybrid microarrays have a relatively low surface coverage difference before/after actuation, and the letters are not clear as was the case for VA microarrays (Figure S20c,c′, Supporting Information). The arbitrarily patterned magnetic actuation modes are also reversible and durable over 100 actuation cycles without any permanent deformation, demonstrating potential applications in magnetocryptograms.

3.3. Directed Liquid Spreading and 3D Self-Assembly of Micropillar Arrays. The instantaneous and reversible changes in surface topology enable on-demand directed liquid spreading at ambient conditions. Liquid pinning and spreading on micropillars are determined by a balance between the contact angle (θ_{eq}) of the solution and the angle between two adjacent posts (θ_p), as shown in Figure 4.[37] θ_p is calculated using the height of the micropillar (H) and the interpillar spacing (l) by the following equation: $\theta_p = \arctan\frac{H}{l}$. The liquid is pinned when $\theta_{eq} > \theta_p$ (Figure 4a), and it spreads when $\theta_p \geq \theta_{eq}$ (Figure 4b). The contact angle of the polymeric solution to PDMS is approximately 73°. Before applying the magnetic field, the aqueous dye solution is pinned on the VA microarray because the interpillar spacing ($l_0 \approx 34$ μm) causes θ_p to be larger than the contact angle. When the magnetic field is applied, the solution begins to spread on the bent VA microarrays because of capillary wicking on the textured surface with a significantly decreased interpillar spacing ($l \approx 5$ μm), reducing θ_p below the contact angle. The switching between the two distinct modes is visualized in Figure 4c and Movie S8, Supporting Information As shown in Figure 4d, the liquid is pinned initially for 7 s and spreads from 7 to 13 s when the external magnetic field is applied. Once the magnetic field is removed, liquid spreading promptly stops. Then, the liquid continues to spread when the magnetic field is applied again. These two regimes coincide with the times when the angle between two posts (θ_p) is greater than the contact angle (θ_{eq}). This on-demand spatiotemporal regulation of liquid spreading opens opportunities for a complex and dynamic modulation of liquid−surface interactions without the need to modify the surface chemistry.

Finally, reversible capillary-assisted 3D self-assembly of micropillars into complex 3D architectures[38,39] is demonstrated by the in situ submersion of polymeric solutions and evaporation of solvents during magnetoactuation (Figure 5). For elastic micropillars with radius r, height h, interpillar

https://dx.doi.org/10.1021/acsami.0c01511
ACS Appl. Mater. Interfaces 2020, 12, 17113−17120

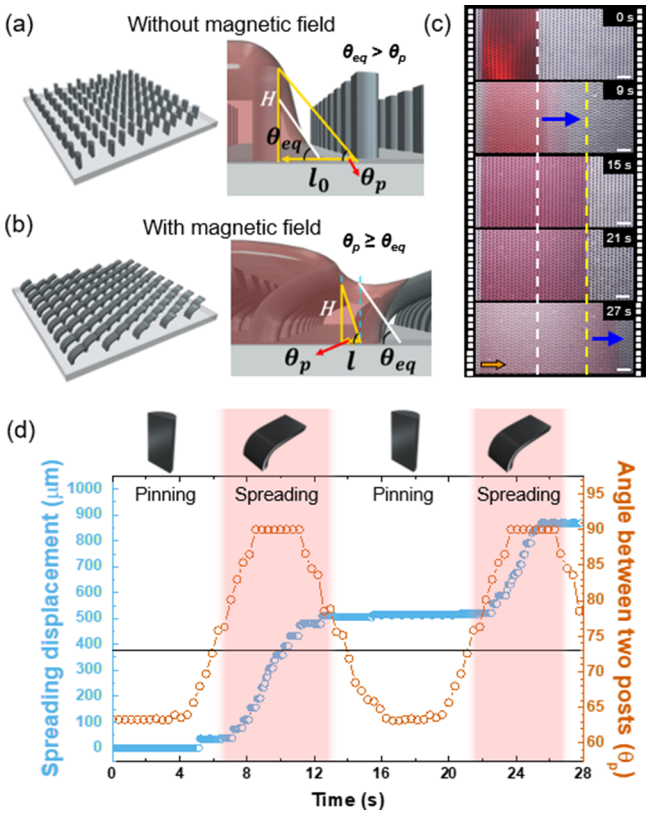

Figure 4. On-demand liquid spreading on the reconfigurable microtextures. (a,b) Schematic image of VA microarray (a) without and (b) with an external magnetic field, and change of interspace between micropillars (l_0: initial interpillar distance, l: interpillar distance after actuation). (c) Captured image of on-demand liquid spreading over time in VA mode (white line: starting line, yellow line: pinned boundary when removing the external magnetic field) (scale bars: 200 μm). (d) Spreading displacement over time (red color region peach square: bending; blue circle: spreading displacement; brown circle: angle between two posts).

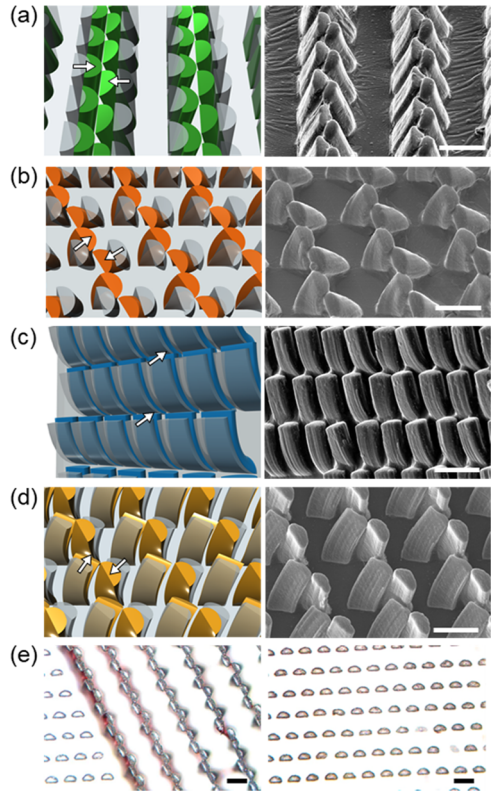

Figure 5. Three-dimensional self-assembled microstructures with the introduction of a different magnetoactuation. (Left) 3D schematic microstructures before and after self-assembly during actuation and (right) SEM images of solute-assisted self-assembled microarrays in each actuation mode. (a) HSA microarray, (b) HLA microarray, (c) VA microarray, (d) hybrid microarray, (e) self-assembled microstructure of the HLA microarray without magnetic field (left), and the microstructure after the polymeric binder is washed out using deionized water (right) (scale bars: 50 μm).

distance d, and Young's modulus E, bending stiffness $k = 3EI/L^3$, and polymeric solutions are pinned at the edges of the micropillars by interfacial tension (γ). As the solvent evaporates, the height of the solution becomes lower than the height of the micropillar, generating lateral capillary forces ($F_C \approx \gamma r$). In the case of nanopillars, the lateral capillary force (F_C) is sufficient to overcome the force to bend two adjacent pillars to come in contact ($F_B \approx kd/h^3$), resulting in an irreversible collapse of the pillars.[34] The micropillars used in this study do not undergo such irreversible deformation as the capillary forces are not sufficient to cause the collapse of the microarrays (r: 15 μm, h: 60 μm, d: 34 μm, E: 0.2 MPa, γ: 3.5 mN/m). To immobilize the self-assembled 3D microstructure, the actuated arrays were submerged in a polymeric solution containing maltodextrin, and then the solution was allowed to evaporate. A thin polymeric layer remains after evaporation and acts as a binder to hold together the self-assembled micropillars, allowing the fabrication of novel 3D microstructures and preserving their geometry even after the removal of the actuating magnetic fields. Furthermore, this layer of binding polymer can later be removed by spraying or rinsing with an appropriate solvent, allowing the reversal of this assembly process.

Notably, the capillary self-assembly of micropillars along the short axis of semicylinders in an unactuated HSA array is observed after submersion and evaporation. In this case, the capillary forces were sufficient to assemble the pillars as they have lower bending stiffnesses (Figures 5a and S21a, Supporting Information). This capillary self-assembly can be used in conjunction with the magnetoactuation to create even more complex architectures that cannot be achieved with just one technique. For instance, twisted HLA microarrays undergo zipping while being twisted by further bending along the short axis of semicylinders (Figures 5b and S21b, Supporting Information). In the case of the VA microarray, the magnetic bending axis coincides with the capillary-assisted bending axis. Hence, further bending occurs and the micropillars come into contact (Figures 5c and S21c, Supporting Information). For the hybrid arrays, the capillary forces join adjacent actuated pillars in pairs, causing them to come into contact at the tips (Figures 5d and S21d, Supporting Information). These unique 3D architectures would be very challenging to achieve with conventional soft lithography techniques, and the assembled microstructures can be released to return to their original shapes by removing the polymer with an appropriate solvent (Figure 5e).

https://dx.doi.org/10.1021/acsami.0c01511
ACS Appl. Mater. Interfaces 2020, 12, 17113−17120

4. CONCLUSIONS

The magnetoactuation modes of anisotropic micropillars in an array were programmed by controlling the alignment of magnetic particles to achieve synchronized and reversible multimodal actuation (bending, twisting, and combination of bending and twisting) without changing the chemical composition or the micropillar geometry. FEM simulations successfully capture the magnetism-driven deformation mechanics and predict deformed shapes that match the observed experimental results well. Nanoindentation confirmed the influence of the magnetic particle alignment on the resulting anisotropic mechanical properties of the microarrays. Magnetoactuation is demonstrated over large areas (1 cm × 1 cm) and in ambient conditions over 100 actuation cycles without any permanent deformation. Various actuation modes were programmed into a single array by designing a complex 3D magnetic field or by the selective filling and aligning of particles by masking the mold. Last, we demonstrated next-level 3D self-assembled architectures by combining magnetoactuation and capillary self-assembly. In situ submersion and evaporation of polymeric solution bind microstructures together to retain their geometries even after the removal of the actuating magnetic field. This transformation can be reversed by simply dissolving the polymeric binders. Reversible shape reconfiguration of micropillars demonstrated in this work enables on-demand, spatiotemporal regulation of liquid spreading. More broadly, these programmable magnetically active micropillar arrays can be used to modulate other texture-dependent surface properties and can serve as a platform for shape-reconfigurable devices such as tunable THz optics, magnetoactuated cryptograms, switchable microfluidics, dynamic tissue engineering scaffolds, and antifouling/self-cleaning surfaces.

■ ASSOCIATED CONTENT

Supporting Information

The Supporting Information is available free of charge at https://pubs.acs.org/doi/10.1021/acsami.0c01511.

Methodology of finite element analysis; calculation of the bending stiffness through the offset angle between the horizontal short axis of the micropost and applied external magnetic field and the degree of bending; schematic illustration of the preparation of preprogrammed, magnetically responsive microarrays; SEM micrographs of the geometry of microarrays; mechanical properties of each micropillar; 3D schematic illustration of the source of linear magnetic field for actuation; mechanism of uniform actuation with tilt angle in particle alignment; correction factor and procedure for FEM simulation; magnetic hysteresis of actuation in each microarray; actuation angle variation of each microarray; and coverage of each microarray before and after actuation (PDF)

RD microarray (MP4)

HSA microarray (MP4)

HLA microarray (MP4)

VA microarray (MP4)

HLA+VA microarray (MP4)

Concerted microarray (MP4)

Arbitrary patterned microarray (MP4)

On-demand droplet spreading on VA microarray (MP4)

■ AUTHOR INFORMATION

Corresponding Authors

A. John Hart − *Department of Mechanical Engineering and Laboratory for Manufacturing and Productivity, Massachusetts Institute of Technology, Cambridge, Massachusetts 02139, United States;* orcid.org/0000-0002-7372-3512; Email: ajhart@mit.edu

Zahyun Ku − *Materials and Manufacturing Directorate, Air Force Research Laboratory, Wright-Patterson Air Force Base, Ohio 45433, United States*; Email: zahyun.ku.1.ctr@us.af.mil

Jeong Jae Wie − *Department of Polymer Science and Engineering, Inha University, Incheon 22212, South Korea;* orcid.org/0000-0001-7381-947X; Email: wie@inha.ac.kr

Authors

Jisoo Jeon − *Department of Polymer Science and Engineering, Inha University, Incheon 22212, South Korea*

Jeong Eun Park − *Department of Polymer Science and Engineering, Inha University, Incheon 22212, South Korea*

Sei Jin Park − *Physical and Life Sciences Directorate, Lawrence Livermore National Laboratory, Livermore, California 94550, United States*

Sukyoung Won − *Department of Polymer Science and Engineering, Inha University, Incheon 22212, South Korea*

Hangbo Zhao − *Department of Mechanical Engineering and Laboratory for Manufacturing and Productivity, Massachusetts Institute of Technology, Cambridge, Massachusetts 02139, United States;* orcid.org/0000-0001-5229-4192

Sanha Kim − *Department of Mechanical Engineering and Laboratory for Manufacturing and Productivity, Massachusetts Institute of Technology, Cambridge, Massachusetts 02139, United States;* orcid.org/0000-0002-3548-6173

Bong Sup Shim − *Department of Chemical Engineering, Inha University, Incheon 22212, South Korea;* orcid.org/0000-0003-3205-6191

Augustine Urbas − *Materials and Manufacturing Directorate, Air Force Research Laboratory, Wright-Patterson Air Force Base, Ohio 45433, United States*

Complete contact information is available at: https://pubs.acs.org/10.1021/acsami.0c01511

Author Contributions

J.J. designed and performed the experiments and analyzed the data. J.E.P., S.W., S.J.P., and H.Z. performed data analysis. A.J.H., Z.K., and J.J.W. conceived the study and administrated the project and resources. J.J. and J.J.W. wrote the manuscript. All authors discussed the results and edited or commented on the manuscript.

Notes

The authors declare no competing financial interest.

■ ACKNOWLEDGMENTS

The INHA university portion of this work was supported by the AOARD grant FA2386-18-1-4103 funded by the U.S. government (AFOSR/AOARD) and NRF (NRF-2019R1A2C1004559). The AFRL portion of this work was supported by the AOARD grant FA2386-18-1-4104 funded by the U.S. government (AFOSR/AOARD). A.J.H. acknowledges support from the MIT-Skoltech Next Generation Program. A portion of this work was performed at LLNL under the auspices of the US Department of Energy under contract DE-

https://dx.doi.org/10.1021/acsami.0c01511
ACS Appl. Mater. Interfaces 2020, 12, 17113−17120

AC52-07NA27344. J.J.W. thanks Prof. J. E. Ryu at North Carolina State University for providing the Si mold.

REFERENCES

(1) Gibson, J. S.; Liu, X.; Georgakopoulos, S. V.; Wie, J. J.; Ware, T. H.; White, T. J. Reconfigurable Antennas Based on Self-Morphing Liquid Crystalline Elastomers. *IEEE Access* **2016**, *4*, 2340−2348.

(2) Zhao, H.; Wie, J. J.; Copic, D.; Oliver, C. R.; Orbaek White, A.; Kim, S.; Hart, A. J. High-Fidelity Replica Molding of Glassy Liquid Crystalline Polymer Microstructures. *ACS Appl. Mater. Interfaces* **2016**, *8*, 8110−8117.

(3) Cui, J.; Drotlef, D.-M.; Larraza, I.; Fernández-Blázquez, J. P.; Boesel, L. F.; Ohm, C.; Mezger, M.; Zentel, R.; Del Campo, A. Bioinspired Actuated Adhesive Patterns of Liquid Crystalline Elastomers. *Adv. Mater.* **2012**, *24*, 4601−4604.

(4) Yao, Y.; Waters, J. T.; Shneidman, A. V.; Cui, J.; Wang, X.; Mandsberg, N. K.; Li, S.; Balazs, A. C.; Aizenberg, J. Multiresponsive Polymeric Microstructures with Encoded Predetermined and Self-Regulated Deformability. *Proc. Natl. Acad. Sci.* **2018**, *115*, 12950−12955.

(5) Wie, J. J.; Shankar, M. R.; White, T. J. Photomotility of Polymers. *Nat. Commun.* **2016**, *7*, 13260.

(6) Lv, J.-a.; Liu, Y.; Wei, J.; Chen, E.; Qin, L.; Yu, Y. Photocontrol of Fluid Slugs in Liquid Crystal Polymer Microactuators. *Nature* **2016**, *537*, 179−184.

(7) Kizilkan, E.; Strueben, J.; Staubitz, A.; Gorb, S. N. Bioinspired Photocontrollable Microstructured Transport Device. *Sci. Robot.* **2017**, *2*, No. eaak9454.

(8) Gelebart, A. H.; Jan Mulder, D.; Varga, M.; Konya, A.; Vantomme, G.; Meijer, E. W.; Selinger, R. L. B.; Broer, D. J. Making Waves in a Photoactive Polymer Film. *Nature* **2017**, *546*, 632−636.

(9) Ware, T. H.; McConney, M. E.; Wie, J. J.; Tondiglia, V. P.; White, T. J. Voxelated Liquid Crystal Elastomers. *Science* **2015**, *347*, 982−984.

(10) Ma, M.; Guo, L.; Anderson, D. G.; Langer, R. Bio-Inspired Polymer Composite Actuator and Generator Driven by Water Gradients. *Science* **2013**, *339*, 186−189.

(11) Arazoe, H.; Miyajima, D.; Akaike, K.; Araoka, F.; Sato, E.; Hikima, T.; Kawamoto, M.; Aida, T. An Autonomous Actuator Driven by Fluctuations in Ambient Humidity. *Nat. Mater.* **2016**, *15*, 1084−1089.

(12) Shin, B.; Ha, J.; Lee, M.; Park, K.; Park, G. H.; Choi, T. H.; Cho, K.-J.; Kim, H.-Y. Hygrobot: A Self-Locomotive Ratcheted Actuator Powered by Environmental Humidity. *Sci. Robot.* **2018**, *3*, No. eaar2629.

(13) Park, J. E.; Jeon, J.; Cho, J. H.; Won, S.; Jin, H.-J.; Lee, K. H.; Wie, J. J. Magnetomotility of Untethered Helical Soft Robots. *RSC Adv.* **2019**, *9*, 11272−11280.

(14) Hu, W.; Lum, G. Z.; Mastrangeli, M.; Sitti, M. Small-Scale Soft-Bodied Robot with Multimodal Locomotion. *Nature* **2018**, *554*, 81−85.

(15) Kim, Y.; Yuk, H.; Zhao, R.; Chester, S. A.; Zhao, X. Printing Ferromagnetic Domains for Untethered Fast-Transforming Soft Materials. *Nature* **2018**, *558*, 274−279.

(16) Won, S.; Kim, S.; Park, J. E.; Jeon, J.; Wie, J. J. On-Demand Orbital Maneuver of Multiple Soft Robots via Hierarchical Magneto-motility. *Nat. Commun.* **2019**, *10*, 4751.

(17) Sydney Gladman, A.; Matsumoto, E. A.; Nuzzo, R. G.; Mahadevan, L.; Lewis, J. A. Biomimetic 4D Printing. *Nat. Mater.* **2016**, *15*, 413−418.

(18) Palleau, E.; Morales, D.; Dickey, M. D.; Velev, O. D. Reversible Patterning and Actuation of Hydrogels by Electrically Assisted Ionoprinting. *Nat. Commun.* **2013**, *4*, 2257.

(19) Kim, Y. S.; Liu, M.; Ishida, Y.; Ebina, Y.; Osada, M.; Sasaki, T.; Hikima, T.; Takata, M.; Aida, T. Thermoresponsive Actuation Enabled by Permittivity Switching in an Electrostatically Anisotropic Hydrogel. *Nat. Mater.* **2015**, *14*, 1002−1007.

(20) Drotlef, D.-M.; Blümler, P.; Del Campo, A. Magnetically Actuated Patterns for Bioinspired Reversible Adhesion (Dry and Wet). *Adv. Mater.* **2014**, *26*, 775−779.

(21) Yang, Z.; Park, J. K.; Kim, S. Magnetically Responsive Elastomer-Silicon Hybrid Surfaces for Fluid and Light Manipulation. *Small* **2018**, *14*, 1702839.

(22) Lin, Y.; Hu, Z.; Zhang, M.; Xu, T.; Feng, S.; Jiang, L.; Zheng, Y. Magnetically Induced Low Adhesive Direction of Nano/Micropillar Arrays for Microdroplet Transport. *Adv. Funct. Mater.* **2018**, *28*, 1800163.

(23) Zhu, Y.; Antao, D. S.; Xiao, R.; Wang, E. N. Real-Time Manipulation with Magnetically Tunable Structures. *Adv. Mater.* **2014**, *26*, 6442−6446.

(24) Drotlef, D.-M.; Blümler, P.; Papadopoulos, P.; Del Campo, A. Magnetically Actuated Micropatterns for Switchable Wettability. *ACS Appl. Mater. Interfaces* **2014**, *6*, 8702−8707.

(25) Baik, S.; Kim, D. W.; Park, Y.; Lee, T.-J.; Ho Bhang, S.; Pang, C. A Wet-Tolerant Adhesive Patch Inspired by Protuberances in Suction Cups of Octopi. *Nature* **2017**, *546*, 396−400.

(26) Autumn, K.; Liang, Y. A.; Hsieh, S. T.; Zesch, W.; Chan, W. P.; Kenny, T. W.; Fearing, R.; Full, R. J. Adhesive Force of a Single Gecko Foot-Hair. *Nature* **2000**, *405*, 681−685.

(27) Li, J.; Hou, Y.; Liu, Y.; Hao, C.; Li, M.; Chaudhury, M. K.; Yao, S.; Wang, Z. Directional Transport of High-Temperature Janus Droplets Mediated by Structural Topography. *Nat. Phys.* **2016**, *12*, 606−612.

(28) Lee, S. G.; Lim, H. S.; Lee, D. Y.; Kwak, D.; Cho, K. Tunable Anisotropic Wettability of Rice Leaf-Like Wavy Surfaces. *Adv. Funct. Mater.* **2013**, *23*, 547−553.

(29) Zhao, H.; Park, S. J.; Solomon, B. R.; Kim, S.; Soto, D.; Paxson, A. T.; Varanasi, K. K.; Hart, A. J. Synthetic Butterfly Scale Surfaces with Compliance-Tailored Anisotropic Drop Adhesion. *Adv. Mater.* **2019**, *31*, 1807686.

(30) Kim, J. H.; Kang, S. M.; Lee, B. J.; Ko, H.; Bae, W. G.; Suh, K. Y.; Kwak, M. K.; Jeong, H. E. Remote Manipulation of Droplets on a Flexible Magnetically Responsive Film. *Sci. Rep.* **2015**, *5*, 17843.

(31) Chu, K.-H.; Xiao, R.; Wang, E. N. Uni-Directional Liquid Spreading on Asymmetric Nanostructured Surfaces. *Nat. Mater.* **2010**, *9*, 413−417.

(32) Chen, H.; Zhang, L.; Zhang, Y.; Zhang, P.; Zhang, D.; Jiang, L. Uni-Directional Liquid Spreading Control on a Bio-Inspired Surface from the Peristome of Nepenthes Alata. *J. Mater. Chem. A* **2017**, *5*, 6914−6920.

(33) Zhang, M.; Wang, L.; Hou, Y.; Shi, W.; Feng, S.; Zheng, Y. Controlled Smart Anisotropic Unidirectional Spreading of Droplet on a Fibrous Surface. *Adv. Mater.* **2015**, *27*, 5057−5062.

(34) Pokroy, B.; Kang, S. H.; Mahadevan, L.; Aizenberg, J. Self-Organization of a Mesoscale Bristle into Ordered, Hierarchical Helical Assemblies. *Science* **2009**, *323*, 237−240.

(35) Ghosh, S.; Tehrani, M.; Al-Haik, M.; Puri, I. Patterning the Stiffness of Elastomeric Nanocomposites by Magnetophoretic Control of Cross-Linking Impeder Distribution. *Materials* **2015**, *8*, 474−485.

(36) Park, S. J.; Zhao, H.; Kim, S.; De Volder, M.; John Hart, A. Predictive Synthesis of Freeform Carbon Nanotube Microarchitectures by Strain-Engineered Chemical Vapor Deposition. *Small* **2016**, *12*, 4393−4403.

(37) Courbin, L.; Denieul, E.; Dressaire, E.; Roper, M.; Ajdari, A.; Stone, H. A. Imbibition by Polygonal Spreading on Microdecorated Surfaces. *Nat. Mater.* **2007**, *6*, 661−664.

(38) De Volder, M.; Hart, A. J. Engineering Hierarchical Nanostructures by Elastocapillary Self-Assembly. *Angew. Chem., Int. Ed.* **2013**, *52*, 2412−2425.

(39) Tawfick, S. H.; Bico, J.; Barcelo, S. Three-Dimensional Lithography by Elasto-Capillary Engineering of Filamentary Materials. *MRS Bull.* **2016**, *41*, 108−114.

https://dx.doi.org/10.1021/acsami.0c01511
ACS Appl. Mater. Interfaces 2020, 12, 17113−17120